

# **Dongming Gan**

Mem. ASME School of Engineering Technology, Polytechnic Institute, Purdue University, West Lafayette, IN 47906 e-mail: dgan@purdue.edu

# Jiaming Fu

School of Engineering Technology, Polytechnic Institute. Purdue University, West Lafayette, IN 47906 e-mail: fu330@purdue.edu

# Han Lin

School of Engineering Technology, Polytechnic Institute, Purdue University, West Lafayette, IN 47906 e-mail: lin853@purdue.edu

# Haoguang Yang

School of Engineering Technology. Polytechnic Institute, Purdue University, West Lafayette, IN 47906 e-mail: yang1510@purdue.edu

# Mo Rastgaar

School of Engineering Technology, Polytechnic Institute, Purdue University, West Lafayette, IN 47906 e-mail: rastgaar@purdue.edu

# **Bvuna-Cheol Min**

Department of Computer and Information Technology, Polytechnic Institute, Purdue University, West Lafayette, IN 47906 e-mail: minb@purdue.edu

# Richard Voyles

School of Engineering Technology, Polytechnic Institute, Purdue University. West Lafayette, IN 47906 e-mail: rvoyles@purdue.edu

# **Actuation-Coordinated Mobile Parallel Robots With Hybrid Mobile and Manipulation Functions**

Mobile robots with manipulation capability are a key technology that enables flexible robotic interactions, large area covering and remote exploration. This paper presents a novel class of actuation-coordinated mobile parallel robots (ACMPRs) that utilize parallel mechanism configurations and perform hybrid moving and manipulation functions through coordinated wheel actuators. The ACMPRs differ with existing mobile manipulators by their unique combination of the mobile wheel actuators and the parallel mechanism topology through prismatic joint connections. Common motion of the wheels will provide mobile function while their relative motion will actuate the parallel manipulation function. This new concept reduces actuation requirement and increases manipulation accuracy and mobile motion stability through coordinated and connected wheel actuators comparing with existing mobile parallel manipulators. The relative wheel location on the base frame also enables a reconfigurable base size with variable moving stability on the ground. The basic concept and general type synthesis are introduced and followed by kinematics and inverse dynamics analysis of a selected three limb ACMPR. A numerical simulation also illustrates the dynamics model and the motion property of the new mobile parallel robot (MPR) followed by a prototype-based experimental validation. The work provides a basis for introducing this new class of robots for potential applications in surveillance, industrial automation, construction, transportation, human assistance, medical applications, and other operations in extreme environment such as nuclear plants, Mars, etc.

[DOI: 10.1115/1.4053821]

Keywords: mechanism design, mobile robots, parallel platforms

## 1 Introduction

Mobile robots [1] are a class of robots that can navigate in a relatively larger area comparing with their body size, which provides desired features including flexibility and area covering. This can work in the environment both with and without human. The former includes manufacturing plants, shopping malls, museums, and other human living zones while the latter includes field areas, space, deep seas, and other hazardous or human-denied

<sup>1</sup>Corresponding author.

Contributed by the Mechanisms and Robotics Committee of ASME for publication in the JOURNAL OF MECHANISMS AND ROBOTICS. Manuscript received October 15, 2021; final manuscript received February 2, 2022; published online March 24, 2022.

environment. In addition to the mobility function, manipulation provides capability to interact with the environment, such as object manipulation [2], material sampling, bomb disposal, remote teleoperation, etc. Current mobile manipulation systems [3,4] normally consist of a mobile base and an onboard manipulator as in Fig. 1(a) [5]. The onboard manipulators can be both serial robot arms and parallel manipulators [6,7], while the mobile base has many different designs for locomotion capability in both flat and uneven terrains. Fixed-wheel base is quite efficient for flat surface and legged mobile robots as in Fig. 1(b) [8] are more for complex terrains. Recently, wheeled legged mobile robots [9-13] have attracted much attention considering the combined benefits

However, in most mobile manipulation systems, the moving bases and the manipulators are decoupled and have two control

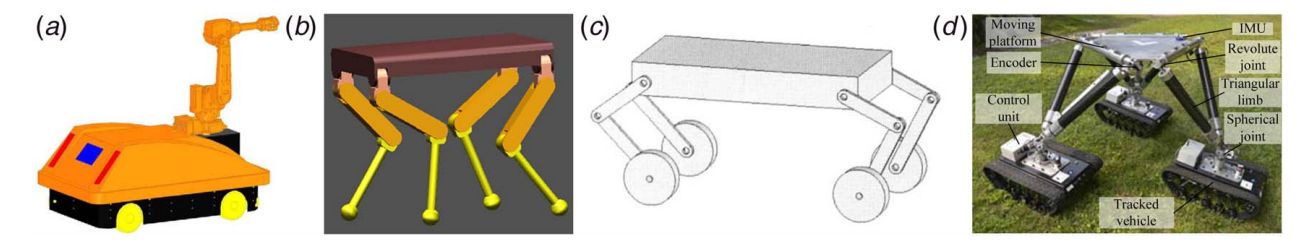


Fig. 1 Different mobile robot manipulators: (a) wheeled [5], (b) legged [8], (c) wheel-legged [14], and (d) mobile parallel robot [15]

systems and hardware structures including actuators, power requirements, and sensors. Mobile parallel robots (MPRs) as in Fig. 1(d)[15] inherit both mobile function of wheeled robots and manipulation capability of parallel robots [7,16–18] with a unified hardware structure and control system using the same set of actuators, sensors, and power supply. The concept of mobile parallel robot was first proposed in Ref. [19] and further investigated on the kinematics and dynamics of a specific design [20]. Then different designs of mobile parallel robots were developed for manipulation [21] and manufacturing [22-24]. Recently, Shentu et al. [25] developed a track-based mobile parallel robot for potential large structure manufacturing. The concept was also extended to multi-robot collaborative manipulation with wheeled mobile bases and connected manipulators [12,26-28]. Each mobile base is an omnidirectional mobile ground vehicle, and they are physically connected by the top structure to form a parallel robot topology. The combined motion of the mobile bases provides the hybrid moving and manipulation function.

Existing mobile parallel robots have separated mobile bases and require each mobile base to be self-supported and stable for operation. Their platform manipulation needs extra accurately coordinated sensing among all mobile bases to have updated mechanism configuration state. Their non-coordinated limbs also bring errors easily to the whole system due to their free relative motion. Considering all those, this paper proposes a new class of mobile parallel robots with coordinated actuations of the mobile bases. The wheeled mobile bases are connected to the frame through prismatic joints which actuate the manipulation through their relative motion. The key feature of the new mobile robots lies on this hybrid topology with coordinated actuation for more stable mobile motion and accurate platform manipulation.

In the following, this paper introduces the concept in Sec. 2 with qualitative comparisons with existing mobile robots. Mobility analysis and type synthesis are presented in Sec. 3 followed by detailed kinematics in Sec. 4 and inverse dynamics modeling in Sec. 5 of a selected 3-limb ACMPR. A numerical example is illustrated in Secs. 6 and 7 illustrates a prototype with experimental configuration validation. Finally, Sec. 8 makes up the conclusions and future work on more detailed modeling and application-oriented designs.

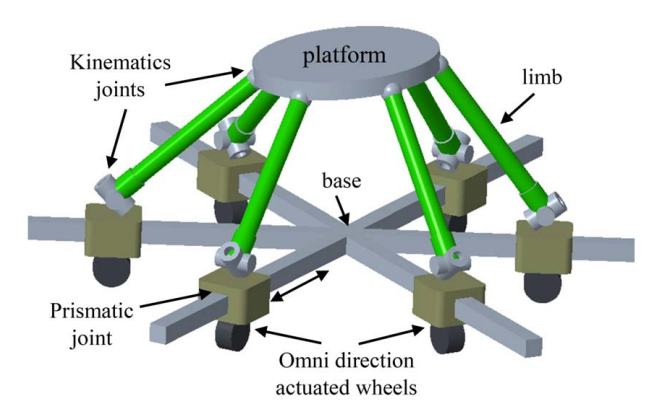


Fig. 2 Concept of the ACMPR (illustrated by a specific 6-mPUS)

## 2 Concept and Comparisons

2.1 The ACMPR Concept. As in Fig. 2, the proposed ACMPRs consist of a base, a platform, multi-limbs that connect to the platform through various kinematics joints and to the base with prismatic joints, and actuated omnidirectional wheels attached to the prismatic joints to support the base on the ground. The combined prismatic joint and the actuated wheel are defined as mobile prismatic (mP) joint. The illustrated example in Fig. 2 uses universal joints to connect the limb to the mP joint and spherical joints to the platform. Thus, it is represented as 6-mPUS with the underlined mP as the actuated joint. Based on this system, the ACMPRs can have mobile function and manipulation function with the wheels as actuation input. When all the wheels move in the same direction and speed, the whole robot will move in that direction to have the mobile motion including translations on the ground and the rotation perpendicular to the ground. When the wheels move along the prismatic joint directions with respect to the base, the platform will be actuated for the manipulation function. In general, hybrid motion will be controlled through the wheels with their common motion to determine the mobile work and their relative motion along the prismatic joints to control the manipulation.

2.2 The Actuated Wheel Options. In this new concept, to realize the hybrid mobile and manipulation functions, the actuated wheels play an important role. With respect to the base, the wheels need to be able to move in omni directions parallel to the base plane. To satisfy this, a minimum setup could be the steered actuated wheel as in Fig. 3(a) in which the actuated wheel can be steered into different directions through a vertical revolute joint perpendicular to the base plane. Similarly, the steered castor wheel can be also used but there will be a resistance force during the offset-axis steering rotation [29]. Theoretically, the ideal wheel could be the spherical wheels which are omnidirectional with point contact to the ground as in Fig. 3(b). Differential drive with two wheels can be also used but with turning constraint as in Fig. 3(c). A more stable and sophisticated solution can be an omnidirectional moving vehicle as the one composed of three omni wheels in Fig. 3(d). Four omni-wheel designs are also popular for mobile ground vehicles [28]. The cost of the omni-wheel actuation is energy consumption due to the multiactuated wheels in one limb in the new concept.

**2.3 Comparison With Existing Mobile Manipulator Concepts.** To better understand the characteristics of the newly proposed mobile parallel robots, a comparison is made below in Table 1 with those related concepts covering both mobile and manipulation functions, especially with parallel robot structures. To make it clear, the comparison is quite general and qualitative by considering their mechanism configurations and structures only.

The first two types are the ones with a mobile base and onboard serial or parallel manipulators. They both have decoupled mobile and manipulation actuation, redundant actuators, and high manipulation accuracy. Except specially designed mobile bases with adjustable wheels, they normally have fixed mobile base footprint with fixed moving stability. The main difference is that the PMMs have much higher payload and stiffness thanks to their multi-loop parallel

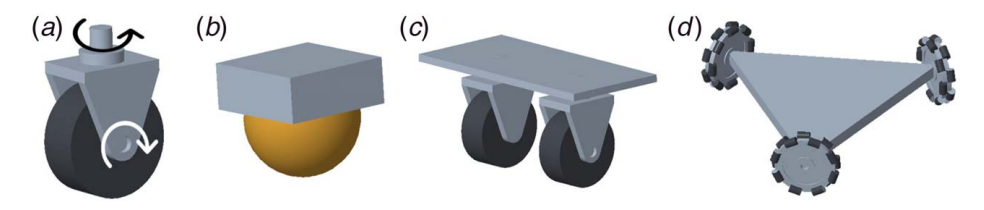


Fig. 3 Possible actuated wheels: (a) steered wheel, (b) spherical wheel, (c) differential drive, and (d) omni wheels

mechanism structures than the SMMs. The former's weakness of small workspace can be compensated by the mobile function but the SMMs may still have better dexterity for a fixed-point manipulation. The proposed ACMPRs are closer to the existing mobile parallel robots (MPRs) considering their parallel robot structures with mobile base actuation for coupled mobile and manipulation functions. They both can have minimum actuation requirement with six actuators for six output platform DOFs and redundant actuators for better stability and controllability by using omnidirectional vehicles. They can have higher payload and stiffness than SMMs but may have less payload than PMMs due to their ground actuation. Between them, the ACMPRs can have higher payload and stiffness than the MPRs if their prismatic joints are locked to form a rigid mobile platform to reduce ground friction requirement. With coordinated actuation through prismatic joints on the base, manipulation accuracy of ACMPRs can be as high as SMMs and PMMs, and better than MPRs of which the manipulation accuracy relies on the relative motion among the ground actuators. While control could be complex for any manipulators, relatively speaking based on Table 1. SMMs and PMMs have low control complexity due to their decoupled mobile and manipulation function. On the other side, MPRs have more complex control requirement due to the coupled motion but ACMPRs reduce the complexity based on their coordinated actuators. Both ACMPRs and MPRs can adjust their base sizes for better maneuver stability but ACMPRs will not have internal limb collision thanks to their coordinated limb configurations. This will also make the motion planning easier than the existing MPRs.

## 3 Mobility Analysis and Type Synthesis

Mobile bases of the ACMPRs provide the ground motion with three DOFs including two translations on the ground plane and

one rotation perpendicular to it through either nonholonomic or holonomic wheel motion. Apart from this, the upper system from the prismatic joints to the platform can be taken as a traditional parallel mechanism with prismatic joints as actuators on the base. Thus, the platform's output mobility is the combination of the base and the parallel mechanism mobilities, which can be complementary to each other or redundant. Based on this, the type synthesis task will be mainly on the parallel mechanisms that have base prismatic actuators. This is a quite loose requirement and will lead to a large number of possible parallel mechanisms that can be used for ACMPRs. The existing rich literature results on type synthesis of all kinds of parallel mechanisms, such as pure translation PMs [32], pure rotation PMs [33,34], 1T2R PMs [35], etc., can be options. This work will not attempt to summarize all those but give a very generally guided synthesis and enumeration of possible limb types with a prismatic joint as the start connection from the base to the platform.

There can be two to six or more limbs in an ACMPR with correspondingly the same number of actuated wheels. To have a stable standing support on the ground, a minimum of three supports are needed. Thus, when there are three or more limbs that are not coplanar or in parallel planes, the above actuated wheels in Fig. 3 are enough for stable support and movement. A special consideration is given to the cases with planar two and three limbs as examples in Fig. 4. Figure 4(a) shows the configuration of a single-loop 2-mPRR planar linkage with 1-DOF upper platform motion and three-wheel support for the 3-DOF ground motion. Since this is a planar case, a single-steered wheel in Fig. 3(a) for each limb is not enough for a stable support and minimum three wheels are needed. Thus, one steered wheel in the right actuated limb and a differential drive in the left limb provide a solution to form a stable plane support in Fig. 4(a). Similarly, for the planar 3-mPRR mobile robot in Fig. 4(b), minimum four steered wheels are needed with two of them in parallel planes. Using the

Table 1 Qualitative comparison with related mobile manipulators

	Serial mobile manipulator (SMM) [5]	Parallel mobile manipulator (PMM)	Mobile parallel robots (MPRs) in the literature [28]	ACMPRs (this work)	
Mobile function versus manipulation	Decoupled	Decoupled	Coupled	Coupled	
Quantity of actuators versus	[30]: 10, 6	[7]: 7, 6	[20,25]: 6, 6	3, 4 (planar case)	
operational DOF of the end-effector	[31]: 11, 6	[6]: 5, 6 (2 redundant)	[28]: 12, 6	4, 5 (planar case) N, 6 ( $N \ge 6$ , N-6 redundant)	
Payload	Low	High	Intermediate	Intermediate or high (with prismatic joint locking)	
Manipulation accuracy	High	High	Low	High	
Control complexity	Low	Low	High	Low	
Stiffness	Low	High	Intermediate	High	
Adjustable base (related to mobile stability)	No (Yes for specially designed mobile bases)	No (Yes for specially designed mobile bases)	Yes	Yes	
Limb collision	NA	NA	Yes	No	

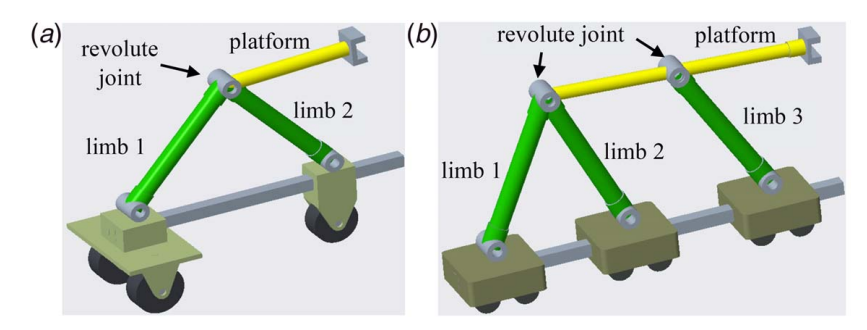


Fig. 4 Planar ACMPRs: (a) 4-DOF mobile 2-mPRR and (b) 5-DOF mobile 3-mPRR

omnidirectional vehicle in Fig. 3(d) for each limb should give more stable control and support as shown in Fig. 4(b). Thus, with the base prismatic joints as actuators, any linkages satisfying this actuation requirement can be used for ACMPRs. Some examples are listed in Table 2 in which only single-loop ones are listed. Any other linkages with multi-loops, for example, 6-bar linkages, 8-bar linkages, and many others with prismatic joints as the base actuators are design options for given applications.

For noncoplanar parallel mechanisms with three or more limbs, possible limb types can be enumerated in Table 2 below. Due to the large number of possibilities of various limb designs, only some of the limbs are listed as examples based on a nonredundant limb representation,  $\underline{mPX_1X_2...X_{n-1}}$ . The underlined mP is the starting actuated prismatic joint and  $X_i$  represents a basic 1-DOF joint including P, R, and screw joints. The 1-DOF joints, P and R, can form the Spherical (S) joint, Universal (U) joint, and Cylindrical (C) joint as listed in the examples.

Based on Table 2, any combination of three or more of those limbs can be assembled to construct new ACMPRs. For example, for an ACMPR with three limbs and 6-DOF platform motion, Fig. 5(a) shows one of the possible structures with two <u>mPUR</u> and one <u>mPRS</u> limbs. The upper parallel mechanism part provides two rotational and one translational DOFs to complement the planar mobility of the base to have a total six-DOF system. The actuated mobile wheels are illustrated with redundant omni-vehicles in Fig. 5(a) which has nine actuators and six platform output DOFs. Figure 5(b) illustrates another example with 3 <u>mPRS</u> limbs in symmetrical platform connections and the upper parallel mechanism has similar three DOFs with that in Fig. 5(a). Three actuated steered wheels are used as the minimum actuation solution making the robot six output platform DOFs with six actuators.

In Secs. 4–7, the 3-limb ACMPR in Fig. 5(*b*) will be used as an example to demonstrate kinematics and dynamics modeling with a trajectory planning illustration for this new class of mobile manipulation robots.

#### 4 Kinematics of an ACMPR With Three mPRS Limbs

**4.1 Basic Geometric Constraints.** The studied ACMPR 3-mPRS mobile robot consists of three PRS limbs on the top with

the platform, a triangular base, and three steered wheels under the base as in Fig. 6. The three spherical joints are symmetrically arranged on the platform while the three prismatic joint directions are equally distributed on the base plane with 120 deg between each other. A global coordinate system O-xyz is set on the ground plane and a moving base coordinate system  $O_b$ - $x_by_bz_b$  is attached to the base geometric center. The  $z_b$ -axis is perpendicular to the base plane and the  $y_b$ -axis passes by the revolute joint center in limb 1. Another moving coordinate system  $O_p$ - $x_p y_p z_p$  is set on the platform with point  $O_p$  at the geometric center of the platform, the  $z_p$ -axis perpendicular to the platform plane and the  $y_p$ -axis passing by the spherical joint center in limb 1. Let  $A_i$  represent the spherical joint center in limb i with  ${}^{p}a_{i}$  the position vector of  $A_i$  expressed in the platform coordinate system,  $B_i$  represent the revolute joint center in limb i with  ${}^{b}\boldsymbol{b}_{i}$  the position vector of  $B_{i}$ expressed in the base coordinate system. The limb length between points  $A_i$  and  $B_i$  is constant and qual for all three limbs with value l.

Based on the above setup, basic geometric constraints of the robot kinematics can be given as

$$\begin{cases} \mathbf{b}_{i} = \mathbf{R}_{z}^{b} t_{i} d_{i} + \mathbf{p}_{1} \\ (\mathbf{R}_{z}(\mathbf{R}_{xy}^{p} \mathbf{a}_{i} + \mathbf{p}_{2}) + \mathbf{p}_{1} - \mathbf{b}_{i})^{2} = l^{2} \\ (\mathbf{R}_{z}(\mathbf{R}_{xy}^{p} \mathbf{a}_{i} + \mathbf{p}_{2}) + \mathbf{p}_{1} - \mathbf{b}_{i})^{T} (\mathbf{R}_{z}^{b} \mathbf{u}_{i}) = 0 \\ b t_{i} = \mathbf{Rot}_{z}((i-1)2\pi/3) \begin{bmatrix} 1 & 0 & 0 \end{bmatrix}^{T} \\ b \mathbf{u}_{i} = \mathbf{Rot}_{z}((i-1)2\pi/3) \begin{bmatrix} 0 & -1 & 0 \end{bmatrix}^{T} \end{cases}$$
(1)

where  $b_i = (b_{ix}, b_{iy}, 0)$  and  $p_1 = (p_{1x}, p_{1y}, 0)$  are the position vectors of points  $B_i$  and  $O_b$  in the global coordinate system,  ${}^bt_i$  is the unit vector along the prismatic joint axis and  ${}^bu_i$  is the unit vector along the revolute joint axis in limb i in the base coordinate system,  $d_i$  is the distance from the prismatic slider center to the center  $O_b$ ,  $\mathbf{R}_z$  is the z-axis rotation matrix of the base coordinate  $O_b$  - $x_by_bz_b$  with respect to the global coordinate system,  $\mathbf{p}_2 = (p_{2x}, p_{2y}, p_{2z})$  is the position vector of the platform coordinate center  $O_p$  described in the base coordinate system,  $\mathbf{R}_{xy}$  is the rotation matrix of the platform coordinate system with respect to the base coordinate system with a 2-DOF rotation about x- and y-axis,  $\mathbf{Rot}((i-1)$   $2\pi/3)$  is the z-axis rotation matrix with rotation angle (i-1)  $2\pi/3$  for limb i.

Table 2 Possible mechanism and limb types

	Mechanism DOFs	Mechanism type	Example mechanisms
Planar PMs	1 DOF 2 DOF 3 DOF	Single-loop Single-loop Multi-loop	<u>mP</u> RRR, <u>mP</u> RRP, <u>mP</u> RPR <u>mP</u> RRRmP 3- <u>mP</u> RR, 3- <u>mP</u> PR, 3- <u>mP</u> PP
Limb for nonplanar PMs	Limb DOFs n DOF (n = 1, 2,, 6)	Limb type $\underline{mP}X_1X_2X_{n-1}$	Example limbs 1 DOF: mP 2 DOF: mPR, mPP 3 DOF: mPRR, mPRP, mPPR, mPPP, mPU, mPC 4 DOF: mPRRR, mPS, mPRU, mPPRR, mPRRP 5 DOF: mPRRRR, mPRS, mPUU, mPPS, mPCU 6 DOF: mPRRRRR, mPUS, PSU, mPRUU, mPRCO

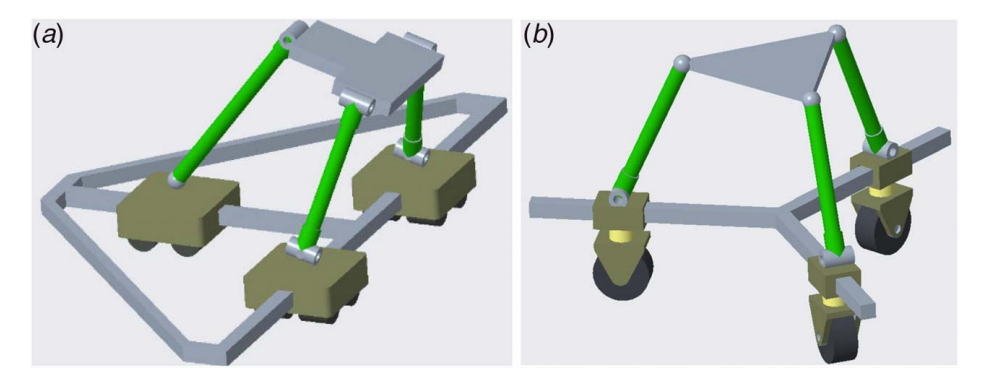


Fig. 5 Nonplanar ACMPRs: (a) mobile 2-mPUR-1-mPSR with mobile bases and (b) mobile 3-mPRS with steered wheels

The first equation in Eq. (1) represents that the position vector of the revolute joint center is transformed from the base coordinate system to the global coordinate by a *z*-axis rotation with a translation on the *xy* plane of the global coordinate system. The second equation is the constant length constraint between the spherical joint center and the revolute joint center while the last one is the geometric constraint that the spherical joint center can only move in the plan perpendicular to the revolute joint axis in each limb.

**4.2 Inverse Kinematics.** The inverse kinematics is to solve the actuation inputs,  $b_i$ , based on given platform orientation  $\mathbf{R} = \mathbf{R}_z \mathbf{R}_{xy}$  and position  $\mathbf{p} = \mathbf{p}_1 + \mathbf{R}_z \mathbf{p}_2$  which are both with respect to the global coordinate system. From the geometric constraints in Eq. (1), there is

$$\begin{cases} (\mathbf{R}^{p}\boldsymbol{a}_{i} + \boldsymbol{p} - \boldsymbol{b}_{i})^{2} = l^{2} \\ (\mathbf{R}^{p}\boldsymbol{a}_{i} + \boldsymbol{p})^{T} (\mathbf{R}_{z}^{b}\boldsymbol{u}_{i}) = -\boldsymbol{b}_{i}^{T} (\mathbf{R}_{z}^{b}\boldsymbol{u}_{i}) \end{cases}$$
  $(i = 1, 2, 3)$  (2)

which gives two constraints in each limb for the two unknowns of  $b_i = (b_{ix}, b_{iy}, 0)$ . The first equation in (2) is a quadratic polynomial of the unknown  $(b_{ix}, b_{iy})$ , while the second equation is linear in these variables. Two solutions can be obtained and they are two intersecting points between a circle centered at the spherical joint center  $A_i$  with radius l and the prismatic joint line. Physically only one of them is feasible considering the continuous motion of the robot.

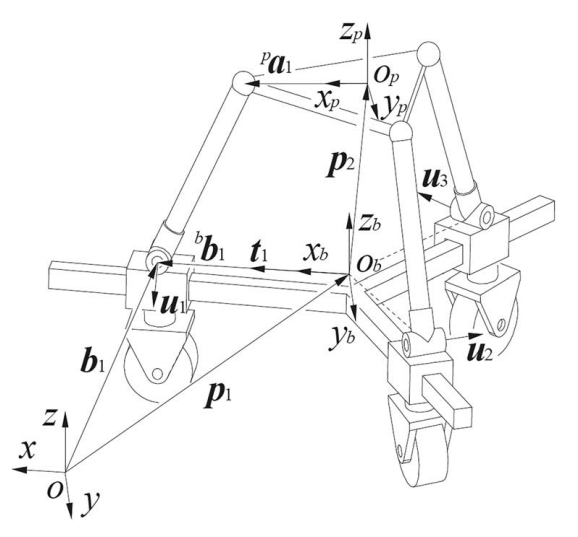


Fig. 6 The kinematics model of the 3-mPRS

**4.3 Forward Kinematics.** In forward kinematics, actuation inputs,  $b_i$ , are known and the platform position p and orientation  $\mathbf{R}$  need to be solved. Based on the position relationship in Eq. (1), there are

$$\mathbf{b}_i = \mathbf{R}_z^b \mathbf{t}_i d_i + \mathbf{p}_1 \quad (i = 1, 2, 3)$$
 (3)

in which the six equations will solve six unknowns including  $p_1 = (p_{1x}, p_{1y}, 0)$ , the orientation angle  $\theta$  of  $\mathbf{R}_z$ , and the three  $d_i$ . In the global coordinate, there is also

$$\begin{cases} t_1 = \frac{\boldsymbol{b}_1 - \boldsymbol{p}_1}{\|\boldsymbol{b}_1 - \boldsymbol{p}_1\|} = (t_{1x}, t_{1y}, 0) \\ \theta = \operatorname{a} \tan 2(t_{1y}, t_{1x}) + \pi/2 \end{cases}$$
(4)

where atan2 (·) is the arctan2 function. Then the forward kinematics problem of the 3-mPRS is changed to the forward kinematics of a 3-PRS parallel mechanism with known prismatic joint inputs  $d_i$ . A similar strategy to the one in Ref. [36] can be used to express the spherical joint center by the limb as  $a_i = b_i + ls_i$  and the three spherical joint centers form the platform triangle with constraint  $(\sqrt{3}\mathbf{r_a})^2 = (a_i - a_j)^T(a_i - a_j)$ . Solving these three constraint equations give 16 solutions of the forward kinematics. For continuous motion, only one of them is the feasible solution for a given trajectory.

# 5 Inverse Dynamics Analysis

**5.1** The Jacobian Matrix. By taking derivatives of Eq. (2) and defining  $s_i$  as the unit vector along the limb  $B_iA_i$ , there is

$$\begin{cases}
2(\mathbf{R}^{p}\boldsymbol{a}_{i} + \boldsymbol{p} - \boldsymbol{b}_{i})^{T}(\boldsymbol{w} \times \mathbf{R}^{p}\boldsymbol{a}_{i} + \dot{\boldsymbol{p}} - \dot{\boldsymbol{b}}_{i}) \\
= 2l\boldsymbol{s}_{i}^{T}(\boldsymbol{w} \times \mathbf{R}^{p}\boldsymbol{a}_{i} + \dot{\boldsymbol{p}} - \dot{\boldsymbol{b}}_{i}) = 0 & (i = 1, 2, 3) \\
(\boldsymbol{w} \times \mathbf{R}^{p}\boldsymbol{a}_{i} + \dot{\boldsymbol{p}} - \dot{\boldsymbol{b}}_{i})^{T}(\mathbf{R}_{z}^{b}\boldsymbol{u}_{i}) + l\boldsymbol{s}_{i}^{T}(\boldsymbol{w}_{z} \times \mathbf{R}_{z}^{b}\boldsymbol{u}_{i}) = 0
\end{cases} (5)$$

where  $\boldsymbol{\omega} = (\omega_x, \omega_y, \omega_z)^{\mathrm{T}}$  is the angular velocity of the platform with respect to the global coordinate system,  $\boldsymbol{\omega}_z = (0, 0, \omega_z)^{\mathrm{T}}$  is the z-axis angular velocity vector. By separating velocities  $\dot{\boldsymbol{b}}_i$  to the right sides of the equations, there is

$$\begin{cases} (\mathbf{R}^{p} a_{i} \times s_{i})^{T} w + s_{i}^{T} \dot{\boldsymbol{p}} = s_{i}^{T} \dot{\boldsymbol{b}}_{i} \\ (i = 1, 2, 3) \end{cases} (6)$$

$$(\mathbf{R}^{p} a_{i} \times \mathbf{R}_{z}^{b} u_{i})^{T} w + (\mathbf{R}_{z}^{b} u_{i} \times \mathbf{l} s_{i})^{T} w_{z} + (\mathbf{R}_{z}^{b} u_{i})^{T} \dot{\boldsymbol{p}} = (\mathbf{R}_{z}^{b} u_{i})^{T} \dot{\boldsymbol{b}}_{i}$$

By rearranging the six equations of all three limbs in (6) into matrix form, it becomes

$$\begin{bmatrix} (\mathbf{R}^{p}\boldsymbol{a}_{1} \times \mathbf{s}_{1})^{T} & \mathbf{s}_{1}^{T} \\ (\mathbf{R}^{p}\boldsymbol{a}_{2} \times \mathbf{s}_{2})^{T} & \mathbf{s}_{2}^{T} \\ (\mathbf{R}^{p}\boldsymbol{a}_{3} \times \mathbf{s}_{3})^{T} & \mathbf{s}_{3}^{T} \\ (\mathbf{R}^{p}\boldsymbol{a}_{1} \times \mathbf{R}_{z}^{b}\boldsymbol{u}_{1})^{T} + (0, 0, (\mathbf{R}_{z}^{b}\boldsymbol{u}_{1} \times l\mathbf{s}_{1})^{T}\boldsymbol{z}) & (\mathbf{R}_{z}^{b}\boldsymbol{u}_{1})^{T} \\ (\mathbf{R}^{p}\boldsymbol{a}_{2} \times \mathbf{R}_{z}^{b}\boldsymbol{u}_{2})^{T} + (0, 0, (\mathbf{R}_{z}^{b}\boldsymbol{u}_{2} \times l\mathbf{s}_{2})^{T}\boldsymbol{z}) & (\mathbf{R}_{z}^{b}\boldsymbol{u}_{2})^{T} \\ (\mathbf{R}^{p}\boldsymbol{a}_{3} \times \mathbf{R}_{z}^{b}\boldsymbol{u}_{3})^{T} + (0, 0, (\mathbf{R}_{z}^{b}\boldsymbol{u}_{3} \times l\mathbf{s}_{3})^{T}\boldsymbol{z}) & (\mathbf{R}_{z}^{b}\boldsymbol{u}_{3})^{T} \end{bmatrix} \begin{bmatrix} \boldsymbol{u} \\ \boldsymbol{p} \end{bmatrix} = \begin{bmatrix} \boldsymbol{s}_{1}^{T} & \boldsymbol{s}_{2}^{T} & \boldsymbol{s}_{3}^{T} \\ (\mathbf{R}_{z}^{b}\boldsymbol{u}_{1})^{T} & \boldsymbol{s}_{3}^{T} \\ (\mathbf{R}_{z}^{b}\boldsymbol{u}_{2})^{T} & (\mathbf{R}_{z}^{b}\boldsymbol{u}_{3})^{T} \end{bmatrix} \begin{bmatrix} \dot{\boldsymbol{b}}_{1} \\ \dot{\boldsymbol{b}}_{2} \\ \dot{\boldsymbol{b}}_{3} \end{bmatrix}$$

$$(7)$$

which can be represented as

$$\mathbf{J}_{A} \begin{bmatrix} \mathbf{w} \\ \dot{\mathbf{p}} \end{bmatrix} = \mathbf{J}_{B} \begin{bmatrix} \dot{\mathbf{b}}_{1} \\ \dot{\mathbf{b}}_{2} \\ \dot{\mathbf{b}}_{3} \end{bmatrix}$$
 (8)

where  $J_A$  and  $J_B$  are the Jacobian matrices.  $J_A$  has the dimension  $6 \times 6$  while  $J_B$  is  $6 \times 9$  in (7). Considering  $b_i = (b_{ix}, b_{iy}, 0)$ , the z-component of  $\dot{b}_i$  can be removed. Thus,  $J_B$  is effectively  $6 \times 6$ . Equation (8) is the mapping between the platform velocity and the actuated mobile base velocities. One side can be solved by knowing the other side and the inverse of  $J_A$  or  $J_B$  when they are not in singular configurations. When  $J_A$  and  $J_B$  are rank-deficient, the mapping between the input and output velocities will be singular and the mechanism will be in singular configurations.

5.2 Velocity Analysis. From Eq. (8), when the mechanism is not in singular configuration, the input velocity can be obtained

$$\begin{bmatrix} \dot{\boldsymbol{b}}_1 \\ \dot{\boldsymbol{b}}_2 \\ \dot{\boldsymbol{b}}_3 \end{bmatrix} = \mathbf{J}_B^{-1} \mathbf{J}_A \begin{bmatrix} \boldsymbol{w} \\ \dot{\boldsymbol{p}} \end{bmatrix}$$
 (9)

For each limb, the vector equation of the spherical joint center can be expressed from both the limb and platform as

$$\mathbf{b}_i + l\mathbf{s}_i = \mathbf{R}^p \mathbf{a}_i + \mathbf{p} \quad (i = 1, 2, 3)$$
 (10)

Taking derivative of the above equation gives

$$\dot{\boldsymbol{b}}_i + l\boldsymbol{w}_i \times \boldsymbol{s}_i = \boldsymbol{w} \times \mathbf{R}^p \boldsymbol{a}_i + \dot{\boldsymbol{p}} \quad (i = 1, 2, 3)$$

Cross-multiplying both sides of (11) with  $t_i$  that is perpendicular to  $w_i$  solves the link angular velocity

$$\mathbf{w}_i = \frac{1}{l\mathbf{t}_i^T \mathbf{s}_i} \mathbf{t}_i \times (\mathbf{w} \times \mathbf{R}^p \mathbf{a}_i + \dot{\mathbf{p}} - \dot{\mathbf{b}}_i)$$

$$= \frac{1}{it_{i}^{T} \mathbf{s}_{i}} \begin{bmatrix} 0 & -t_{iz} & t_{iy} \\ t_{iz} & 0 & -t_{ix} \\ -t_{iy} & t_{ix} & 0 \end{bmatrix} \begin{pmatrix} \mathbf{J}_{ai} \mathbf{J}_{A}^{-1} \mathbf{J}_{B} - \begin{bmatrix} \frac{(3-i)(2-i)}{2} & 0 & 0 \\ 0 & (3-i)(i-1) & 0 \\ 0 & 0 & \frac{(i-1)(i-2)}{2} \end{bmatrix} \end{pmatrix} \begin{bmatrix} \dot{\mathbf{b}}_{1} \\ \dot{\mathbf{b}}_{2} \\ \dot{\mathbf{b}}_{3} \end{bmatrix} = \mathbf{J}_{wi} \begin{bmatrix} \dot{\mathbf{b}}_{1} \\ \dot{\mathbf{b}}_{2} \\ \dot{\mathbf{b}}_{3} \end{bmatrix}$$
(12)

The center of mass of link  $B_iA_i$  is taken as the geometric center of the link and its position vector is expressed as  $\mathbf{p}_{ci} = \mathbf{b}_i + l\mathbf{s}_i/2 = (\mathbf{R}^p a_i + \mathbf{p} + \mathbf{b}_i)/2$ . Then its derivative gives the velocity

$$\dot{\boldsymbol{p}}_{ci} = (\boldsymbol{w} \times \mathbf{R}^p \boldsymbol{a}_i + \dot{\boldsymbol{p}} + \dot{\boldsymbol{b}}_i)/2$$

$$= \frac{1}{2} \left( \mathbf{J}_{ai} \mathbf{J}_{A}^{-1} \mathbf{J}_{B} + \begin{bmatrix} \frac{(3-i)(2-i)}{2} & 0 & 0 \\ 0 & (3-i)(i-1) & 0 \\ 0 & 0 & \frac{(i-1)(i-2)}{2} \end{bmatrix} \right) \begin{bmatrix} \dot{\boldsymbol{b}}_{1} \\ \dot{\boldsymbol{b}}_{2} \\ \dot{\boldsymbol{b}}_{3} \end{bmatrix} = \mathbf{J}_{pi} \begin{bmatrix} \dot{\boldsymbol{b}}_{1} \\ \dot{\boldsymbol{b}}_{2} \\ \dot{\boldsymbol{b}}_{3} \end{bmatrix}$$
(13)

On the base, each limb has  $b_i = p_1 + d_i t_i$  and its derivative shows

$$\dot{b}_i = \dot{p}_1 + \dot{d}_i t_i + d_i w_z \times t_i \quad (i = 1, 2, 3)$$
(14)

Combining three equations in (14) in matrix form, there is

$$\begin{bmatrix} w_{z} \\ \dot{p}_{1x} \\ \dot{p}_{1y} \\ \dot{d}_{1} \\ \dot{d}_{2} \\ \dot{d}_{3} \end{bmatrix} = \begin{bmatrix} (d_{1}z \times t_{1})_{x} & 1 & 0 & t_{1x} & 0 & 0 \\ (d_{1}z \times t_{1})_{y} & 0 & 1 & t_{1y} & 0 & 0 \\ (d_{2}z \times t_{2})_{x} & 1 & 0 & 0 & t_{2x} & 0 \\ (d_{2}z \times t_{2})_{y} & 0 & 1 & 0 & t_{2y} & 0 \\ (d_{3}z \times t_{3})_{x} & 1 & 0 & 0 & 0 & t_{3x} \\ (d_{3}z \times t_{3})_{x} & 1 & 0 & 0 & 0 & t_{3} \end{bmatrix}^{-1} \begin{bmatrix} \dot{b}_{1} \\ \dot{b}_{2} \\ \dot{b}_{3} \end{bmatrix} = \mathbf{J}_{b1}^{-1} \begin{bmatrix} \dot{b}_{1} \\ \dot{b}_{2} \\ \dot{b}_{3} \end{bmatrix}$$

$$(15)$$

where  $z = (0, 0, 1)^{T}$ ,  $\mathbf{J}_{b1}$  is a  $6 \times 6$  matrix and its inverse exists. Then the base velocity can be expressed as

$$\begin{bmatrix} \mathbf{w}_{z} \\ \dot{\mathbf{p}}_{1} \end{bmatrix} = \begin{bmatrix} 0 \\ 0 \\ w_{z} \\ \dot{p}_{1x} \\ \dot{p}_{1y} \\ 0 \end{bmatrix} = \begin{bmatrix} 0_{1\times6} \\ 0_{1\times6} \\ \mathbf{J}_{b1}^{-1}(row1) \\ \mathbf{J}_{b1}^{-1}(row2) \\ \mathbf{J}_{b1}^{-1}(row3) \\ 0_{1\times6} \end{bmatrix} \begin{bmatrix} \dot{\mathbf{b}}_{1} \\ \dot{\mathbf{b}}_{2} \\ \dot{\mathbf{b}}_{3} \end{bmatrix} = \mathbf{J}_{b} \begin{bmatrix} \dot{\mathbf{b}}_{1} \\ \dot{\mathbf{b}}_{2} \\ \dot{\mathbf{b}}_{3} \end{bmatrix}$$
(16)

Table 3 Parameters of the 3mPRS

Items	Mass (kg)	Inertia (kg m <sup>2</sup> )	Size (m)
Platform Limb	1 0.5	Diag [0.01, 0.01, 0.02] Diag [0.0038, 0.0038, 0.0001]	$r_a = 0.18$ l = 0.5
Base frame	2	Diag [0.02, 0.02, 0.04]	$r_b = 0.6$

**5.3** Acceleration Analysis. Taking derivative of the first equation in Eq. (5), there is

$$(\mathbf{w} \times \mathbf{R}^{p} \mathbf{a}_{i} + \dot{\mathbf{p}} - \dot{\mathbf{b}}_{i})^{2} + 2l\mathbf{s}_{i}^{T} (\dot{\mathbf{w}} \times \mathbf{R}^{p} \mathbf{a}_{i} + \mathbf{w} \times (\mathbf{w} \times \mathbf{R}^{p} \mathbf{a}_{i}) + \ddot{\mathbf{p}} - \ddot{\mathbf{b}}_{i}) = 0$$

$$2(\mathbf{w} \times \mathbf{R}^{p} \mathbf{a}_{i} + \dot{\mathbf{p}} - \dot{\mathbf{b}}_{i})^{T} (\mathbf{w}_{z} \times \mathbf{R}_{z}^{b} \mathbf{u}_{i}) + (\dot{\mathbf{w}} \times \mathbf{R}^{p} \mathbf{a}_{i} + \mathbf{w} \times (\mathbf{w} \times \mathbf{R}^{p} \mathbf{a}_{i}) + \ddot{\mathbf{p}} - \ddot{\mathbf{b}}_{i})^{T} (\mathbf{R}_{z}^{b} \mathbf{u}_{i}) +$$

$$l\mathbf{s}_{i}^{T} (\dot{\mathbf{w}}_{z} \times \mathbf{R}_{z}^{b} \mathbf{u}_{i} + \mathbf{w}_{z} \times (\mathbf{w}_{z} \times \mathbf{R}_{z}^{b} \mathbf{u}_{i})) = 0$$

$$(17)$$

Then the actuation acceleration of  $\vec{b}_i$  can be solved linearly based on given platform accelerations  $(\dot{w}, \ddot{p})$ .

Taking further derivatives of Eqs. (11) and (13) shows the acceleration of link  $B_iA_i$  as

$$\ddot{\boldsymbol{b}}_i + l\dot{\boldsymbol{w}}_i \times \boldsymbol{s}_i + l\boldsymbol{w}_i \times (\boldsymbol{w}_i \times \boldsymbol{s}_i) = \dot{\boldsymbol{w}} \times \boldsymbol{R}^p \boldsymbol{a}_i + \boldsymbol{w} \times (\boldsymbol{w} \times \boldsymbol{R}^p \boldsymbol{a}_i) + \ddot{\boldsymbol{p}}$$
(18)

Cross-multiplying both sides of (18) with  $t_i$  that is perpendicular to  $w_i$  solves the link angular acceleration

$$\dot{\mathbf{w}}_i = \frac{1}{lt_i^T \mathbf{s}_i} t_i \times (\dot{\mathbf{w}} \times \mathbf{R}^p \mathbf{a}_i + \mathbf{w} \times (\mathbf{w} \times \mathbf{R}^p \mathbf{a}_i) + \ddot{\mathbf{p}} - \ddot{\mathbf{b}}_i - l\mathbf{w}_i \times (\mathbf{w}_i \times \mathbf{s}_i))$$
(19)

Taking further derivative of Eq. (13) gives the translation acceleration of the center of mass of link  $B_iA_i$ :

$$\ddot{\mathbf{p}}_{ci} = (\dot{\mathbf{w}} \times \mathbf{R}^p \mathbf{a}_i + \mathbf{w} \times (\mathbf{w} \times \mathbf{R}^p \mathbf{a}_i) + \ddot{\mathbf{p}} + \ddot{\mathbf{b}}_i)/2 \tag{20}$$

The derivative of Eq. (14) shows the base acceleration relationship as

$$\ddot{\boldsymbol{b}}_{i} = \ddot{\boldsymbol{p}}_{1} + \ddot{\boldsymbol{d}}_{i}\boldsymbol{t}_{i} + 2\dot{\boldsymbol{d}}_{i}\boldsymbol{w}_{z} \times \boldsymbol{t}_{i} + d_{i}\boldsymbol{w}_{z} \times (\boldsymbol{w}_{z} \times \boldsymbol{t}_{i}) + d_{i}\dot{\boldsymbol{w}}_{z} \times \boldsymbol{t}_{i} \quad (i = 1, 2, 3)$$
(21)

The combined matrix of the three equations in (21) solves the base accelerations

$$\begin{bmatrix} \dot{w}_{z} \\ \ddot{p}_{1x} \\ \ddot{p}_{1y} \\ \ddot{d}_{1} \\ \ddot{d}_{2} \\ \ddot{d}_{3} \end{bmatrix} = \mathbf{J}_{b1}^{-1} \begin{bmatrix} \ddot{b}_{1} - 2\dot{d}_{1}w_{z} \times t_{1} - d_{1}w_{z} \times (w_{z} \times t_{1}) \\ \ddot{b}_{2} - 2\dot{d}_{2}w_{z} \times t_{2} - d_{2}w_{z} \times (w_{z} \times t_{2}) \\ \ddot{b}_{3} - 2\dot{d}_{3}w_{z} \times t_{3} - d_{3}w_{z} \times (w_{z} \times t_{3}) \end{bmatrix}$$
(22)

## 5.4 Inverse Dynamics Using Virtual Work Principle.

Inverse dynamics solves the input force requirements for a given platform configuration with known kinematics and dynamics parameters. Virtual work principle can be used for the 3-mPRS mobile parallel robot based on the above kinematics analysis results and it can be expressed as

$$\delta \boldsymbol{b}^T \mathbf{F}_a + \delta \boldsymbol{x}_p^T \boldsymbol{F}_p + \delta \boldsymbol{x}_b^T \boldsymbol{F}_b + \sum_{i=1}^3 \delta \boldsymbol{x}_i^T \boldsymbol{F}_i = 0$$
 (23)

where  $F_a$  are the actuation forces from all the three mobile bases

$$\boldsymbol{F}_{j} = \begin{bmatrix} \hat{\boldsymbol{n}}_{j} \\ \hat{f}_{j} \end{bmatrix} = \begin{bmatrix} -\mathbf{I}_{j} \dot{\boldsymbol{w}}_{j} - \boldsymbol{w}_{j} \times (\mathbf{I}_{j} \boldsymbol{w}_{j}) \\ m_{j} \boldsymbol{g} - m_{j} \dot{\boldsymbol{v}}_{j} \end{bmatrix}, (j = p, b, 1, 2, 3), \text{ are the}$$

inertia wrenches of the platform, the base and the links  $B_iA_i$ . Corresponding virtual displacement  $\delta x_j$  (j=p, b, 1, 2, 3) can be all expressed by the base displacement  $\delta b$  based on the velocity mappings in Sec. 6.1 as

$$\delta \mathbf{x}_{p} = \mathbf{J}_{A}^{-1} \mathbf{J}_{B} \delta \mathbf{b}, \quad \delta \mathbf{x}_{b} = \mathbf{J}_{b} \delta \mathbf{b}, \quad \delta \mathbf{x}_{i} = \begin{bmatrix} \mathbf{J}_{wi} \\ \mathbf{J}_{pi} \end{bmatrix} \delta b$$
 (24)

Substitute (24) into (23), there is

$$\delta \boldsymbol{b}^{T} (\boldsymbol{F}_{a} + (\mathbf{J}_{A}^{-1} \mathbf{J}_{B})^{T} \boldsymbol{F}_{p} + \mathbf{J}_{b}^{T} \boldsymbol{F}_{b} + \sum_{i=1}^{3} \begin{bmatrix} \mathbf{J}_{wi} \\ \mathbf{J}_{pi} \end{bmatrix}^{T} \boldsymbol{F}_{i}) = 0$$
 (25)

This gives the inverse dynamic solution of the 3-<u>mPRS</u> since (25) works for any virtual displacement

$$\boldsymbol{F}_{a} = -(\mathbf{J}_{A}^{-1}\mathbf{J}_{B})^{T}\boldsymbol{F}_{p} - \mathbf{J}_{b}^{T}\boldsymbol{F}_{b} - \sum_{i=1}^{3} \begin{bmatrix} \mathbf{J}_{wi} \\ \mathbf{J}_{pi} \end{bmatrix}^{T} \boldsymbol{F}_{i}$$
 (26)

## 6 A Numerical Example

To validate the above developed kinematics and dynamics models, a numeral example is simulated in Matlab. The mechanism parameters are selected as in Table 3 in which  $r_b$  is the outer radius of the three-spoke base frame.

The inverse dynamic analysis is based on the input of the platform. Both rotations about x- and y-axis are taking ga = 3 while the rotation about z-axis uses ga = 20 with the same periodic function as the following

$$\begin{cases} \gamma = (ga/2\pi)^2(\sin(2\pi t/ga)) \\ \dot{\gamma} = (ga/2\pi)\cos(2\pi t/ga) \\ \ddot{\gamma} = -\sin(2\pi t/ga) \end{cases}$$
(27)

where t is time. The translations along the x, y, and z directions follow the second-order trajectory  $ma^*t^2$  with magnitude ma = 10, 5, and 0.01, respectively. Those magnitudes also represent their constant accelerations with a scale of two along those directions.

The platform starts from an initial position (0, 0, 0.3) with no orientation. The simulation results are listed in Fig. 7. The traced trajectory of the mobile robot and the platform orientation is shown in Fig. 7(a) which represents a translation of 6m along the *x*-axis and 3m along the *y*-axis of the mobile base starts from the origin (0, 0). The platform shows rotations about all the three axes with a major rotation about the *z*-axis. Based on the given platform trajectory, the three actuated mobile base forces, velocities, and accelerations are

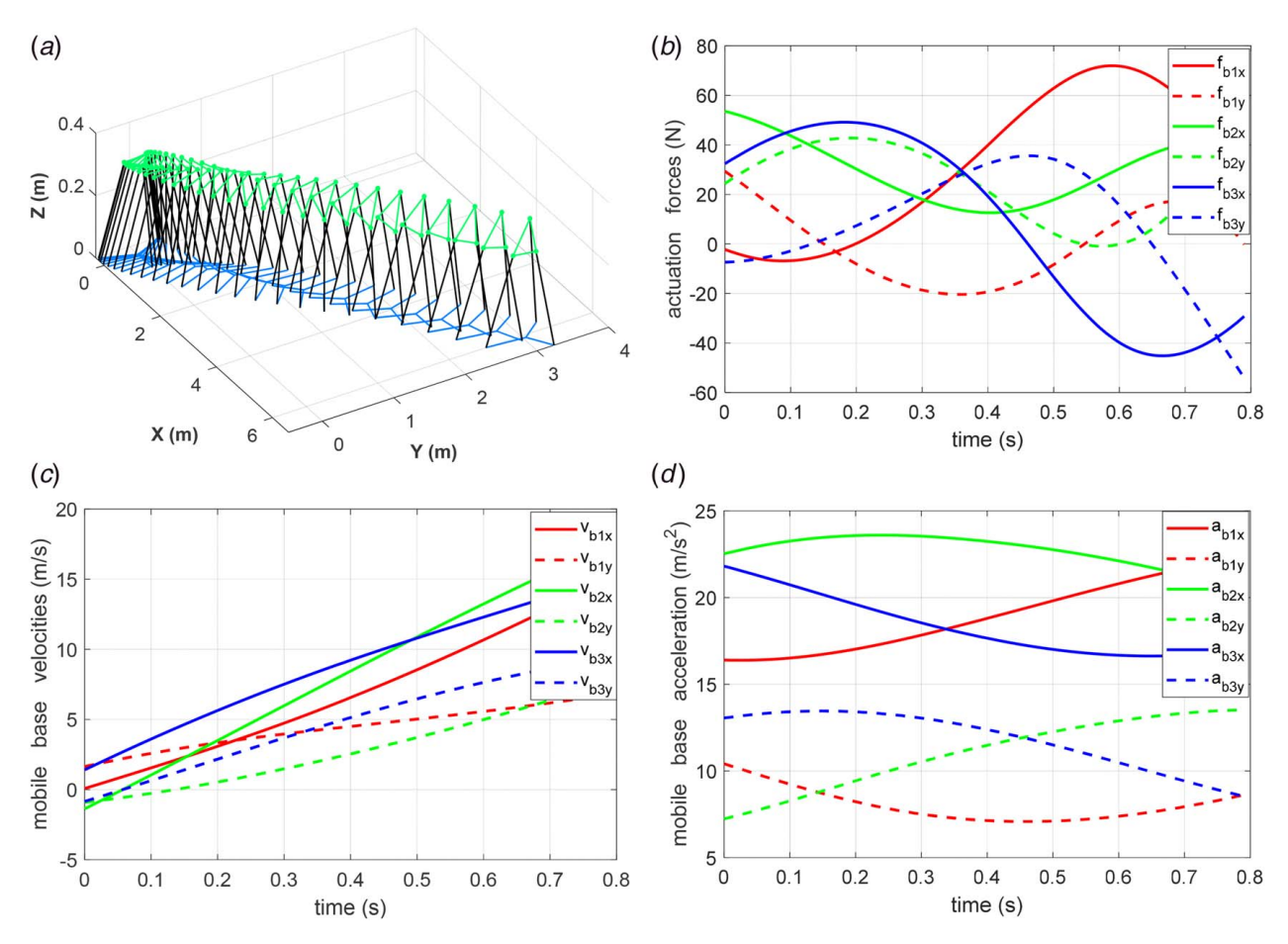


Fig. 7 Simulation results: (a) simulated trajectory, (b) actuation forces of the three mobile bases, (c) velocities of the three mobile bases, and (d) accelerations of the three mobile bases

shown in Figs. 7(b)–7(d) in which the solid lines are for the x direction and dashed lines are for the y direction. An obvious behavior can be seen in Figs. 7(c) and 7(d) that the y direction velocities and accelerations are smaller than those of the x. This is due to the fact that the platform trajectory starts from a zero velocity but the constant acceleration of the x-axis  $(20 \text{ m/s}^2)$  is double the acceleration along y-axis  $(10 \text{ m/s}^2)$ . Based on those constant accelerations, the mobile bases also increase their velocities gradually as in Fig. 7(c) with those positive accelerations as in Fig. 7(d) following the inverse kinematics. The actuation forces are fluctuated with

Spherical joint limb thin tube large tube place of the pl

Fig. 8 Prototype of the 3-mPRS

an increased trend as in Fig. 7(b) due to the increased inertia forces from the velocities.

# 7 Prototyping and Experimental Validation

To validate and further study this new kind of mobile manipulator systems, a prototype of the 3-mPRS has been built based on three omnidirectional mobile robots as in Fig. 8. The omnidirectional holonomic robot provides equivalent actuation to the steered wheel function as in Fig. 6. Each robot has 4 powered caster wheels driven by eight motors with 0.2 mm-resolution encoders to roll and steer independently. Each mobile robot has a dimension of 62 cm × 62 cm and 50 kg payload to provide sufficient support to the base and the sliders. The limbs and the platform are all 3D printed with a revolute pin joint connection on the base and a spherical joint on the platform in each limb. The base prismatic joint is realized by a pair of steel tubes with the smaller one sliding inside the larger tube. The three smaller tubes form the base structure with a connection at the central by a 3D printed pad as in Fig. 8 while the larger tubes are fixed on the mobile robots as sliding tracks. The tube sliding is not a purely prismatic joint connection but a cylindrical joint. This will not affect the mobile parallel mechanism geometric constraints since the mobile bases are assumed moving on a flat ground plane. The tube rotation can also potentially provide flexibility on uneven terrains which will be investigated and tested in the future work.

Due to limited-time setup for the accurate Vicon tracking system in this new lab space, global coordinated testing data were not recorded at this stage. Some preliminary motion testing has been conducted as in Fig. 9. When all the three mobile robots reached the base center to the minimum distance, the upper platform reached the

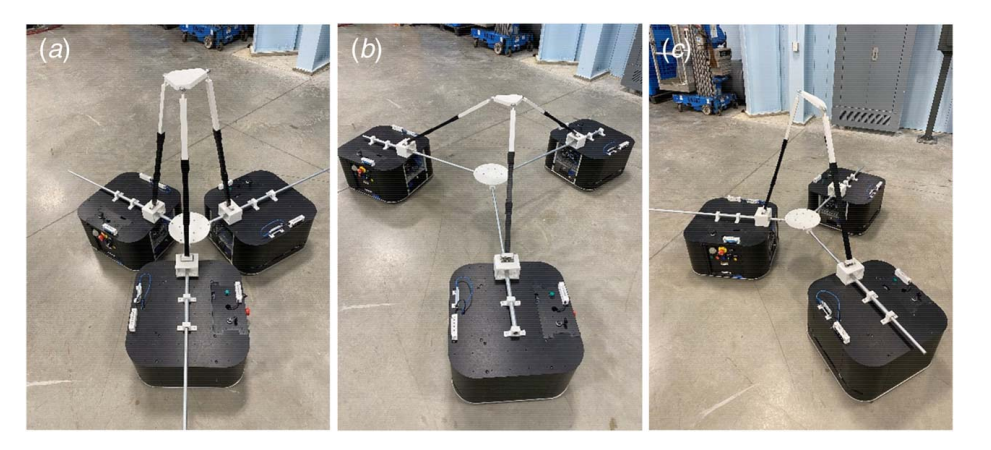


Fig. 9 Translation along the z-axis and orientation tests: (a) maximum z, (b) minimum z, and (c) orientation about y-axis

maximum height along the z-axis which is perpendicular to the ground plane as in Fig. 9(a). When all the three moved away from the base center to the maximum as in Fig. 9(b), the upper platform translated down to its minimum height. This also demonstrated the translation motion along z-axis of the 3-mPRS based on the symmetrical relative motion of the three mobile base robots. While two mobile robots stayed still, the other mobile robot moved along the slider forward and backward, the upper platform oriented about the y-axis as in Fig. 9(c) with an estimated maximum angle 45 deg. This validated the rotation motion of the upper platform.

To demonstrate a more general motion, a hybrid motion was conducted as recorded in Fig. 10. The three robots were simultaneously controlled with a host machine, which calculated the inverse kinematics of the mechanism in real time, and distributed the velocity commands to the three robot bases. In the setup, a 3-degrees-of-freedom joystick was used as human input for the desired velocity vector of the platform. In the current phase of our experiment, combinations of hybrid motions of the manipulator

were tested and translated to the linear and angular velocities of each mobile robot. The experimental result is shown in Fig. 10(a) in which the triangles represent the formation of the three mobile robots and the curved lines are the recorded trajectories. The linear and angular velocities of each robot during the motion were also recorded, as in Fig. 10. The velocities are confined with the desired inverse kinematics of the mechanism based on the joystick input. The motion sequence samples are shown in Fig. 11.

While translation along the z-axis and orientation about x- and y-axis of the upper platform are within limited motion range as in Fig. 9, the translation on the ground and rotation about the z-axis are unlimited as the mobile function. The above tests demonstrated the basic function of this new mobile parallel robot with hybrid manipulation and mobile functions. More accurate and data-based testing will be conducted with the Vicon system. Outdoor testing will be also conducted following the indoor experiment confirmation to explore general application scenarios and requirements.

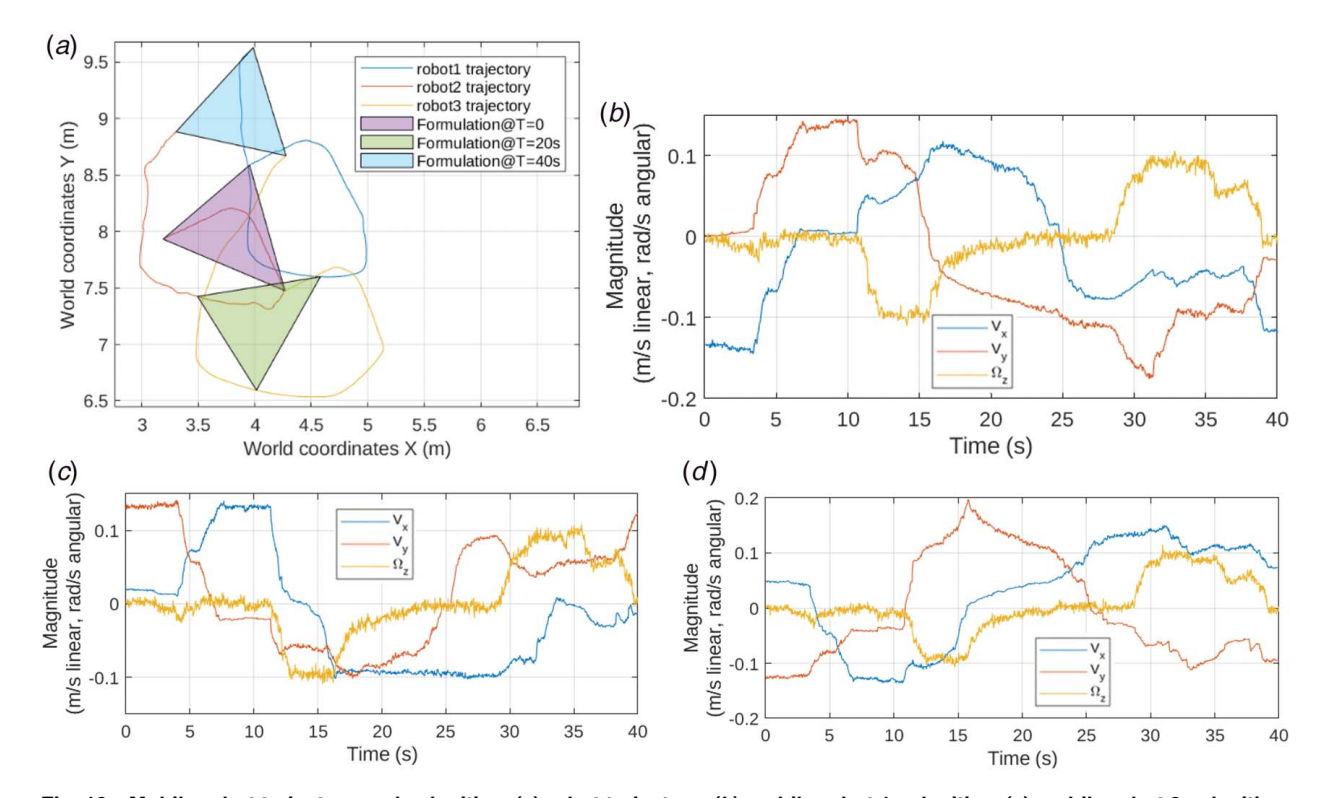


Fig. 10 Mobile robot trajectory and velocities: (a) robot trajectory, (b) mobile robot 1 velocities, (c) mobile robot 2 velocities, and (d) mobile robot 3 velocities

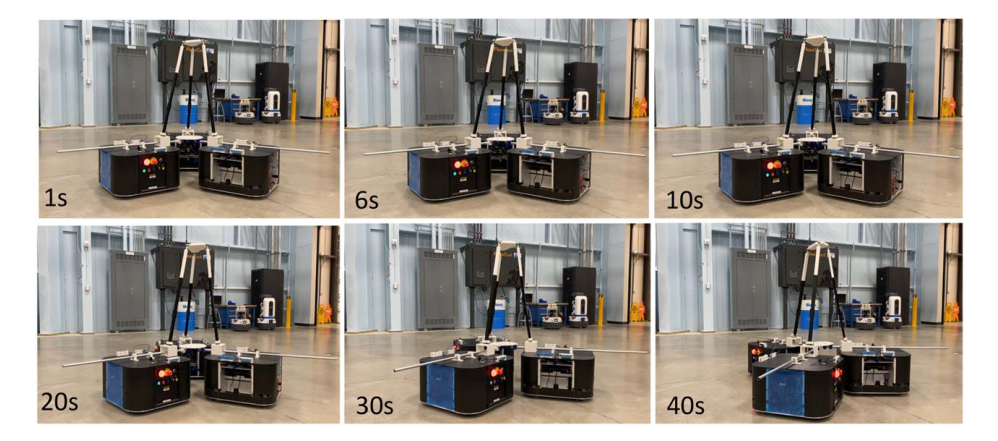


Fig. 11 A general hybrid motion test

#### 8 Conclusions and Future Work

This paper introduced a new class of mobile parallel robots with coordinated actuation bases. The key feature of hybrid mobile and manipulation function was explained with qualitative comparisons with the literature mobile manipulation robots. The new robots added mobile function to the parallel robots and kept their accurate manipulation function based on the mobile prismatic joints on the base frame. Various new mobile parallel robots were synthesized with this new concept and examples were illustrated. Following those, the inverse dynamics of a selected 3-mPRS mobile parallel robot was derived and detailed kinematics relationship between the platform and the mobile bases was investigated. A numerical example was presented to demonstrate the kinematics and dynamics behavior along a given trajectory. The translations along the x- and y-axis, and the rotation about the z-axis were decoupled with the platform orientations about x- and y-axis with translation along the z-axis. A prototype of the 3-mPRS was built and some qualitative testing validated those basic translation and orientation functions. Both the theoretical and experimental results showed that the proposed new mobile parallel robots had easy controllable function features with big potentials in various applications scenarios requiring both mobile and manipulation functions.

The coming work on this topic will focus on the mobile base dynamics and actuation force model. Advanced control and trajectory planning algorithms will be developed to explore more advantages of this new kind of mobile parallel robots with hybrid mobile and manipulation functions. The prototype will be tailored for potential applications including lower-limb prosthesis simulation, logistic warehouse manipulation and transportation, field exploration, etc.

## **Funding Data**

This work was funded in part by the Purdue Polytechnic RDE seed grant project and the National Science Foundation (NSF) grant under FRR-2131711.

#### **Conflict of Interest**

There are no conflicts of interest.

# **Data Availability Statement**

The datasets generated and supporting the findings of this article are obtainable from the corresponding author upon reasonable request. No data, models, or code were generated or used for this paper.

#### References

- Rubio, F., Valero, F., and Llopis-Albert, C., 2019, "A Review of Mobile Robots: Concepts, Methods, Theoretical Framework, and Applications," Int. J. Adv. Robot. Syst., 16(2), pp. 1–22.
- [2] Ciocarlie, M., Hsiao, K., Leeper, A., and Gossow, D., 2012, "Mobile Manipulation Through an Assistive Home Robot," IEEE Int. Conf. Intell. Robot. Syst., pp. 5313–5320.
- [3] Han, Z., Allspaw, J., Lemasurier, G., Parrillo, J., Giger, D., Reza Ahmadzadeh, S., and Yanco, H. A., 2020, "Towards Mobile Multi-Task Manipulation in a Confined and Integrated Environment With Irregular Objects," arXiv. 11025– 11031
- [4] Dömel, A., Kriegel, S., Kaßecker, M., Brucker, M., Bodenmuller, T., and Suppa, M., 2017, "Toward Fully Autonomous Mobile Manipulation for Industrial Environments," Int. J. Adv. Robot. Syst., 14(4), pp. 1–19.
- [5] Song, T., Xi, F., Guo, S., and Lin, Y., 2016, "Optimization of a Mobile Platform for a Wheeled Manipulator," ASME J. Mech. Rob., 8(6), p. 061007.
- [6] Li, Y., Xu, Q., and Liu, Y., 2006, "Novel Design and Modeling of a Mobile Parallel Manipulator," Proc. IEEE Int. Conf. Robot. Autom., pp. 1135–1140.
- [7] Chen, Y., Wang, W., Abdollahi, Z., Wang, Z., Schulte, J., Krovi, V., and Jia, Y., 2018, "A Robotic Lift Assister: A Smart Companion for Heavy Payload Transport and Manipulation in Automotive Assembly," IEEE Robot. Autom. Mag., 25(2), pp. 107–119.
- [8] Ding, X., and Chen, H., 2016, "Dynamic Modeling and Locomotion Control for Quadruped Robots Based on Center of Inertia on SE(3)," ASME J. Dyn. Syst. Meas. Contr., 138(1), p. 011004.
- [9] Geilinger, M., Winberg, S., and Coros, S., 2020, "A Computational Framework for Designing Skilled Legged-Wheeled Robots," IEEE Robot. Autom. Lett., 5(2), pp. 3674–3681.
- [10] Geilinger, M., Poranne, R., Desai, R., Thomaszewski, B., and Coros, S., 2018, "Skaterbots: Optimization-Based Design and Motion Synthesis for Robotic Creatures With Legs and Wheels," ACM Trans. Graph., 37(4), pp. 1–12.
- [11] Zhou, X., Alamdari, A., and Krovi, V., 2013, "Articulated Wheeled Vehicles: Back to the Future?," Mech. Mach. Sci., 14, pp. 227–238.
- [12] Tang, C. P., and Krovi, V. N., 2007, "Manipulability-Based Configuration Evaluation of Cooperative Payload Transport by Mobile Manipulator Collectives," Robotica, 25(1), pp. 29–42.
- [13] Bjelonic, M., Sankar, P. K., Bellicoso, C. D., Vallery, H., and Hutter, M., 2020, "Rolling in the Deep—Hybrid Locomotion for Wheeled-Legged Robots Using Online Trajectory Optimization," IEEE Robot. Autom. Lett., 5(2), pp. 3626–3633.
- [14] Jun, S. K., White, G. D., and Krovi, V. N., 2006, "Kinetostatic Design Considerations for an Articulated Leg-Wheel Locomotion Subsystem," ASME J. Dyn. Syst. Meas. Contr., 128(1), pp. 112–121.
- [15] Liu, X. J., Xie, F., Gong, Z., and Shentu, S., 2018, "Kinematics Analysis and Motion Control of a Mobile Robot Driven by Three Tracked Vehicles," Proc. ASME Des. Eng. Tech. Conf., 5A, pp. 1–9.
- [16] Voyles, R. M., and Larson, A. C., 2005, "TerminatorBot: A Novel Robot With Dual-Use Mechanism for Locomotion and Manipulation," IEEE/ASME Trans. Mechatron., 10(1), pp. 17–25.
- [17] Voyles, R. M., and Godzdanker, R., 2008, "Side-Slipping Locomotion of a Miniature, Reconfigurable Limb/Tread Hybrid Robot," Proc. 2008 IEEE Int. Work, Safety, Secur. Rescue Robot., pp. 58–64.
- [18] Pedemonte, N., Rasheed, T., Marquez-Gamez, D., Long, P., Hocquard, É, Babin, F., Fouché, C., Caverot, G., Girin, A., and Caro, S., 2020, "FASTKIT: A Mobile Cable-Driven Parallel Robot for Logistics," Springer Tracts Adv. Robot., 132, pp. 141–163.
- [19] Ben-Horin, R., Shoham, M., and Djerassi, S., 1998, "Kinematics, Dynamics and Construction of a Planarly Actuated Parallel Robot," Robot. Comput. Integr. Manuf., 14(2), pp. 163–172.
- [20] Horin, P. B., Djerassi, S., Shoham, M., and Horin, R. B., 2006, "Dynamics of a Six Degrees-of-Freedom Parallel Robot Actuated by Three Two-Wheel Carts," Multibody Syst. Dyn., 16(2), pp. 105–121.

- [21] Hu, Y., Zhang, J., Wan, Z., and Lin, J., 2011, "Design and Analysis of a 6-DOF Mobile Parallel Robot With 3 Limbs," J. Mech. Sci. Technol., 25(12), pp. 3215–3222.
- [22] Olarra, A., Allen, J. M., and Axinte, D. A., 2014, "Experimental Evaluation of a Special Purpose Miniature Machine Tool With Parallel Kinematics Architecture: Free Leg Hexapod," Precis. Eng., 38(3), pp. 589–604.
- [23] Sidibe, M. B., Fu, Y. L., and Ma, Y., 2007, "Wheeled Mobile Robot Actuations of a Multiple Degrees-of-Freedom Parallel Manipulator," Proc. WSEAS Int. Conf. Circuits, Syst. Signal Telecommun., pp. 65–70.
- [24] Yang, H., Krut, S., Pierrot, F., and Baradat, C., 2011, "On the Design of Mobile Parallel Robots for Large Workspace Applications," Proc. ASME Des. Eng. Tech. Conf., 6, pp. 767–776.
- [25] Shentu, S., Xie, F., Liu, X. J., and Gong, Z., 2020, "Motion Control and Trajectory Planning for Obstacle Avoidance of the Mobile Parallel Robot Driven by Three Tracked Vehicles," Robotica., 39(6), pp. 1037–1050.
- [26] Kumar, N., and Coros, S., 2020, "Trajectory Optimization for a Class of Robots Belonging to Constrained Collaborative Mobile Agents (CCMA) Family," Proc. IEEE Int. Conf. Robot. Autom., pp. 10391–10397.
- [27] Kumar, N., and Coros, S., 2019, "Optimization Driven Kinematic Control of Constrained Collaborative Mobile Agents With High Mobility," arXiv.
- [28] Kumar, N., and Coros, S., 2019, "An Optimization Framework for Simulation and Kinematic Control of Constrained Collaborative Mobile Agents (CCMA) System," arXiv.

- [29] Siegwart, R., Nourbakhsh, I. R., and Scaramuzza, D., 2011, Introduction to Autonomous Mobile Robots, MIT Press, Cambridge, MA.
- [30] Mobile Manipulator XL-GEN, https://www.roscomponents.com/en/mobile-manipulators/30-xl-gen.html#/gps-no/summit\_xl\_docking\_station-no/encoders-no/cpu-jnf797\_q370\_i3\_8th\_gen\_8gb\_ram\_250gb\_m2\_ssd/omni\_wheels-rubber\_wheels/kinova\_gripper\_options-no/summit\_xl\_rgbd\_zone-no/summit\_xl\_zone\_
- [31] KUKA KMR iiwa, https://www.kuka.com/-/media/kuka-downloads/imported/ 9cb8e311bfd744b4b0eab25ca883f6d3/kuka\_kmriiwa\_en.pdf?rev=cca9122203a 64572bd15791550ca08c2&hash=36AE9386FAF0A0FBE43416080C7D95B1
- [32] Kong, X., 2013, "Type Synthesis of 3-DOF Parallel Manipulators With Both a Planar Operation Mode and a Spatial Translational Operation Mode," ASME J. Mech. Rob., 5(4), p. 041015.
- [33] Kong, X., and Gosselin, C. M., 2004, "Type Synthesis of 3-DOF Spherical Parallel Manipulators Based on Screw Theory," ASME J. Mech. Des., 126(1), pp. 101–108.
- [34] Gan, D., Dai, J. S., and Caldwell, D. G., 2011, "Constraint-Based Limb Synthesis and Mobility-Change-Aimed Mechanism Construction," ASME J. Mech. Des., 133(5), p. 051001.
- [35] Gan, D., Dai, J. S., Dias, J., and Seneviratne, L., 2014, "Constraint-Plane-Based Synthesis and Topology Variation of a Class of Metamorphic Parallel Mechanisms," J. Mech. Sci. Technol., 28(10), pp. 4179–4191.
- [36] Gan, D., Dias, J., and Seneviratne, L., 2016, "Unified Kinematics and Optimal Design of a 3rRPS Metamorphic Parallel Mechanism With a Reconfigurable Revolute Joint," Mech. Mach. Theory, 96, pp. 239–254.